# Reversed voltage-dependent gating of a bacterial sodium channel with proline substitutions in the S6 transmembrane segment

**Yong Zhao*, Todd Scheuer, and William A. Catterall†**

Department of Pharmacology, Mail Stop 357280, University of Washington, Seattle, WA 98195-7280

Contributed by William A. Catterall, November 5, 2004

**Members of the voltage-gated-like ion channel superfamily have a conserved pore structure. Transmembrane helices that line the pore (M2 or S6) are thought to gate it at the cytoplasmic end by bending at a hinge glycine residue. Proline residues favor bending of $\alpha$-helices, and substitution of proline for this glycine (G219) dramatically stabilizes the open state of a bacterial $Na^+$ channel NaChBac. Here we have probed S6 pore-lining residues of NaChBac by proline mutagenesis. Five of 15 proline-substitution mutants yielded depolarization-activated $Na^+$ channels, but only G219P channels have strongly negatively shifted voltage dependence of activation, demonstrating specificity for bending at G219 for depolarization-activated gating. Remarkably, three proline-substitution mutations on the same face of S6 as G219 yielded channels that activated upon hyperpolarization and inactivated very slowly. Studies of L226P showed that hyperpolarization to −147 mV gives half-maximal activation, 123 mV more negative than WT. Analysis of combination mutations and studies of block by the local anesthetic etidocaine favored the conclusion that hyperpolarization-activated gating results from opening of the cytoplasmic gate formed by S6 helices. Substitution of multiple amino acids for L226 indicated that hyperpolarization-activated gating was correlated with a high propensity for bending, whereas depolarization-activated gating was favored by a low propensity for bending. Our results further define the dominant role of bending of S6 in determining not only the voltage dependence but also the polarity of voltage-dependent gating. Native hyperpolarization-activated gating of hyperpolarization- and cyclic nucleotide-gated (HCN) channels in animals and KAT channels in plants may involve bending at analogous S6 amino acid residues.**

excitability | sodium channels | proline mutagenesis | pore-gating

Voltage-gated $Na^+$ channels are large transmembrane proteins that generate and propagate action potentials (1, 2). In eukaryotes, the pore-forming $\alpha$-subunit is composed of four homologous domains containing six probable transmembrane $\alpha$-helices (TM) (S1 to S6; reviewed in ref. 3). The lining of the inner pore is formed by the S6 segments of each domain, and the narrow ion selectivity filter is formed by the P loop in the linker between the S5 and S6 segments (3). The S4 segments of each domain contain positively charged amino acids at every third position that serve as voltage sensors (3). Opening and closing of the pore are controlled by changes in membrane potential (3). The pore is closed at the resting membrane potential and opens in response to depolarization (3). $Na^+$ channels are the founding members of a large family of 143 voltage-gated-like ion channels (4). Their similar pore structures suggest fundamental similarities in pore-gating mechanisms despite the marked differences in their activation by changes in membrane voltage and/or by binding of intracellular messengers like cyclic nucleotides, lipids, and $Ca^{2+}$.

Ion channels discovered in bacteria have provided crucial insights into structure and function of this superfamily. X-ray crystal structures of two bacterial 2-TM $K^+$ channels, KcsA and MthK, have revealed two different conformations of the pore, which is formed by their M2 segments that are analogous in structure and function to the S6 segments of $Na^+$ channels. In the KcsA structure, the pore-lining M2 helices are cylindrical, crossing the membrane at a sharp angle to form a tightly packed helical bundle at the cytoplasmic end of the pore (5). In contrast, in the structure of the distantly related, $Ca^{2+}$-gated MthK channel, the M2 helical bundle is bent at a highly conserved glycine residue and splayed open at the cytoplasmic end (5–7). Bending of the M2 helix at this glycine residue has been proposed as a widespread gating mechanism for the voltage-gated-like superfamily of ion channels (7). The overall pore structure of a bacterial 6-TM voltage-gated $K^+$ channel is similar to 2-TM KcsA and MthK channels (8). These structural studies provide clear but static snapshots of the structures of these channels. Independent functional evidence to support the proposed mechanisms of gating is needed.

A voltage-gated $Na^+$ channel discovered in the halophilic bacterium *Bacillus halodurans* (NaChBac) (9) is a homotetramer of separate 6-TM subunits. It activates in response to depolarization and selectively conducts $Na^+$, but it resembles both $Na^+$ and $Ca^{2+}$ channels in amino acid sequence and may be an ancestor of both eukaryotic proteins (9). Our previous studies of proline-substitution mutants of NaChBac provided functional evidence that the conserved glycine residue in its S6 segment is the gating hinge of the channel (10). Proline residues in $\alpha$-helices favor bends with an average angle of 26° (11, 12), similar to the 30° bend observed in the crystal structure of MthK (7). We found that substitution of proline for the gating-hinge glycine (G219) in the S6 segment of NaChBac dramatically favored the open state of the channel, providing functional evidence that bending at G219 is important for opening the pore (10). In this study, we systematically substituted proline for the native residues in the inner pore-lining segment of the S6 helix of NaChBac. Our results show that substitution of proline for G219 is unique in producing depolarization-activated $Na^+$ channels that open at very negative membrane potentials, providing further support for a key role of this amino acid residue in pore opening. Moreover, we were surprised to find that three proline-substitution mutations, located on the same face of the S6 segment as the gating hinge glycine, transform NaChBac from a depolarization-activated channel into a hyperpolarization-activated channel. These results further emphasize the importance of the bending of the S6 segment in opening the pore and show that these gating movements control both the voltage dependence and the polarity of gating. Our results have interesting implications for the small family of hyperpolarization- and cyclic nucleotide-gated (HCN) channels in animals (13–15) and

Abbreviations: HCN, hyperpolarization- and cyclic nucleotide-gated; KAT, $K^+$ channel from *Arabidopsis thaliana*; TM, transmembrane $\alpha$-helix.

*Present address: Cerep, Inc., 15318 Northeast 95th Street, Redmond, WA 98052.

†To whom correspondence should be addressed. E-mail: wcatt@u.washington.edu.

the $K^+$ channel from *Arabidopsis thaliana* (KAT) in plants (16, 17), whose natural gating is activated by hyperpolarization.

## Experimental Procedures

**Molecular Biology.** NaChBac cDNA (9) was cloned from *Bacillus halodurans* genomic DNA (American Type Culture Collection) into the pCDM8 vector (Invitrogen) by PCR using Pfu DNA polymerase (Stratagene). Site-directed mutagenesis was done by PCR of the full-length plasmid pCDM8/NaChBac cDNA using Pfu polymerase and verified by sequencing.

**Electrophysiological Recording and Data Analysis.** Human embryonic kidney tsA-201 cells were maintained in DMEM/F12 medium (Invitrogen) supplemented with 10% FBS (HyClone) plus 25 units of penicillin and 25 $\mu$g of streptomycin per ml. Cells were cotransfected with NaChBac constructs and a vector encoding human CD8 (EBO-pCD-leu2; American Type Culture Collection) as described in ref. 18. Transiently transfected cells were visualized with polystyrene microspheres precoated with anti-CD8 antibody (Dynabeads M-450 CD8, Dynal, Great Neck, NY) (19).

Whole-cell voltage-clamp experiments were performed on transiently transfected tsA-201 cells at 22°C as described in ref. 20. Etidocaine (AstraZeneca) was dissolved in dimethyl sulfoxide to make a 500 mM stock solution and diluted with extracellular solution to give the indicated concentrations. Data were analyzed using IGOR PRO 4.00 (WaveMetrics, Lake Oswego, OR). Activation–voltage relationships were fit with a Boltzmann function, $1/(1 + \exp((V - V_a)/k))$, where $V_a$ was the voltage for half-maximal activation, and $k$ was a slope factor.

## Results and Discussion

**Effects of Proline Substitutions in the S6 Segment on Depolarization-Activated Gating of NaChBac Channels.** Our previous studies showed that mutation G219P slowed activation and inactivation of the NaChBac channel and greatly shifted its voltage dependence of activation toward more negative potentials, consistent with function of G219 as a key hinge in opening the channel (10) (Figs. 1 and 2*A*). In contrast, substitution of a proline for I218 and T220, which flank G219, had only modest effects on the rates of activation and inactivation and the voltage dependence of activation (10) (Figs. 1 and 2*A*). To assess the effects of substitution of proline residues in the S6 segment more broadly, we have constructed proline mutations for each of the amino acid residues from L217 to I231, whose positions in the S6 $\alpha$-helix are illustrated as a helical net in Fig. 1*A Left*. Mutants F224P and I228P gave substantial inward currents (Fig. 1*A*). For F224P, the rates of activation and inactivation were similar to the WT channel (Fig. 1*A*), and the voltage dependence of activation was shifted only −14 mV, much less than the shift of −52 mV for G219P (10) (Fig. 2*A*). For I228P, only small inward $Na^+$ currents were recorded. They had a voltage dependence of inactivation similar to WT, but we were unable to characterize them quantitatively (Fig. 1*A*). These results show that the substitution of proline for G219 is unique among these five amino acid residues in yielding channels that are functionally expressed and have a marked negative shift in the voltage dependence of activation by depolarizing test pulses.

For $Na^+$ channels that open and do not inactivate by the end of the depolarizing test pulse, repolarization to the holding potential results in tail currents that reflect increased inward $Na^+$ conductance through the open channel because of the greater electrical driving force at −120 mV. Decay of these tail currents provides a measure of the rate of pore closure at −120 mV. For WT and F224P, tail currents recorded after brief depolarizations decay rapidly with time constants of ≈1–3 ms, indicating rapid closure of the pore (10) (Fig. 2*B*). In contrast,

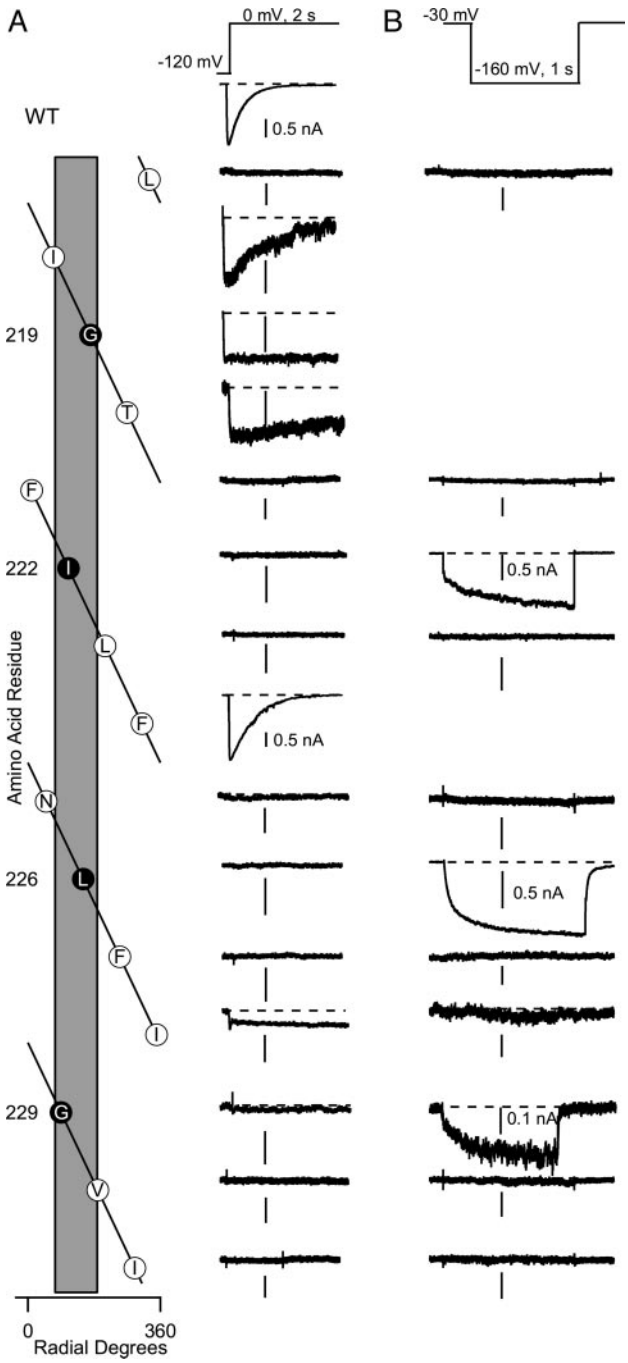


**Fig. 1.** Proline substitutions in the S6 segment of NaChBac. (*A*) The amino acid sequence of the S6 segment of NaChBac is illustrated in *Left* as a helical net, from L217 to I231. The gray bar indicates a 100° radial surface of the $\alpha$-helix on which all mutations that strongly affect gating are located. Depolarization-activated $Na^+$ currents conducted by the WT channel (top) and corresponding proline-substitution mutants at each position in the $\alpha$-helix are illustrated in *Right*. $Na^+$ currents were recorded during test pulses to 0 mV for 2 s from a holding voltage of −120 mV. (*B*) Hyperpolarization-activated $Na^+$ currents conducted by the indicated mutants that did not conduct depolarization-activated currents are illustrated. $Na^+$ currents were recorded during test pulses to −160 mV for 1s from a holding voltage of −30 mV. [Scale bars: 0.2 nA (unless otherwise noted).]

for G219P, closure of the pore was greatly slowed (Fig. 2*B*), with a time constant for pore closure at −120 mV of 260 ms.

Of the total of 15 proline-substitution mutants in the S6 segment that we have studied, 5 resulted in depolarization-

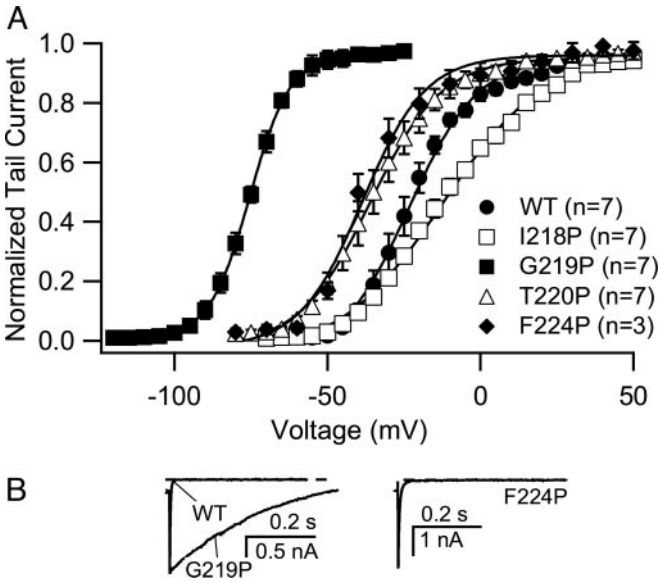


**Fig. 2.** Voltage dependence of activation and rate of pore closure for depolarization-activated proline-substituted channels. (*A*) $Na^+$ currents were activated by depolarizations to the indicated potentials from a holding potential of −120 mV. Peak tail currents were measured after each depolarization, normalized to the maximum current measured, and plotted versus the test pulse potential. (*B*) Time courses of tail currents for WT and the indicated mutant channels.

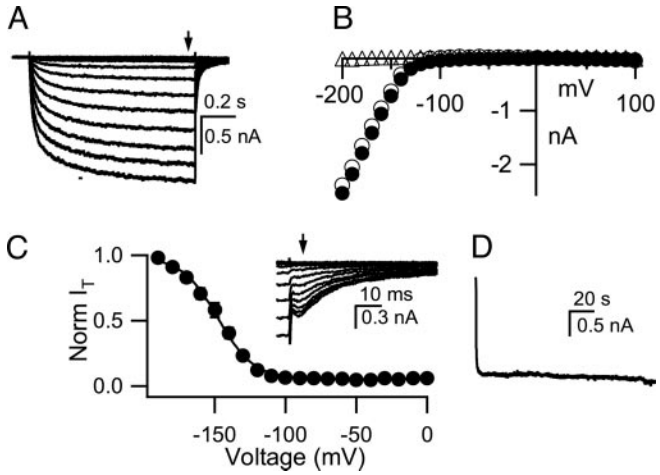


**Fig. 3.** Hyperpolarization-activated gating of the L226P channel. (*A*) Sodium currents recorded from L226P in response to a series of test-pulse potentials from +100 mV to −200 mV in 10-mV steps from a holding voltage of −30 mV. (*B*) *I–V* curves for the L226P channel [with (filled circles) and without (open circles) leak subtraction] and for a cell transfected with empty vector (triangles). The amplitude of currents was measured immediately before the end of the test pulses (arrow in *A*). Leak subtraction used a P/4 protocol at −30 mV. (*C*) Voltage dependence of activation of L226P measured from tail currents. From a holding potential of −30 mV, cells were hyperpolarized for 1s to potentials from +30 mV to −200 mV in 10-mV steps and tail currents were measured after repolarization to −30 mV. The voltage for half-maximal activation ($V_a$) is −147 ± 0.8 mV, with a slope factor of −12.3 ± 0.6 ($n$ = 5). (*Inset*) Example tail currents. (*D*) Time course of $Na^+$ current conducted by the L226P channel during a 2-min hyperpolarizing pulse. From a holding potential of −30 mV, the cell was hyperpolarized to a −160-mV pulse for 2 min.

activated inward $Na^+$ currents (Fig. 1*A*), 7 conducted no detectable $Na^+$ current in response to either depolarizing or hyperpolarizing test pulses (Fig. 1 *A* and *B*), and, to our surprise, 3 mutants conducted hyperpolarization-activated $Na^+$ currents (Fig. 1*B*). The unexpected functional properties of these three mutants are described in the following sections.

**Hyperpolarization-Activated Gating of NaChBac Channels with Proline Substitutions in the S6 Segment.** Among the 143 members of the superfamily of voltage-gated-like ion channels in humans (4), the small family of four HCN channels is unique in activating in response to hyperpolarization but not depolarization (13–15). KAT channels in plants have similar properties (16, 17). In light of the unusual gating properties of the HCN and KAT channels, we tested whether any of our proline substitution mutants could be activated by hyperpolarizing test pulses. Remarkably, hyperpolarization from −30 mV to −160 mV activated inward $Na^+$ currents conducted by mutants I222P, L226P, and G229P (Fig. 1*B*). The inward currents produced by I222P and G229P were too small to analyze quantitatively. However, large currents were observed for L226P, and these were analyzed in detail.

From a holding potential of −30 mV, voltage steps were applied to potentials from +100 mV to −200 mV. No current was observed for steps positive to −100 mV. However, for steps to more negative potentials, striking inward $Na^+$ currents were activated (Fig. 3 *A* and *B*), whose reversal potentials were unchanged from WT (data not shown). The time course of activation was characterized by fast and slow phases (Fig. 3*A*). The slower phase of activation was incomplete in 1 s, and the $Na^+$ currents continued to increase until the end of the 1-s hyperpolarizing test pulses. To determine the voltage dependence of activation of the hyperpolarization-activated $Na^+$ current, the channels were activated by hyperpolarizing test pulses to different potentials, and tail currents were recorded after depolarization back to the holding potential of −30 mV (Fig. 3*C Inset*). The voltage dependence of the peak tail current for each mutant was fitted to a Boltzmann function, yielding a voltage for half-maximal activation ($V_a$) of −147 mV for L226P (Fig. 3*C*), 123 mV more negative than for WT.

In addition to its strong effects on the voltage dependence of activation, mutation L226P also affected inactivation. No inactivation was apparent during 1-s hyperpolarizations to different membrane potentials (Fig. 3*A*), and no inactivation was observed during a 2-min hyperpolarization to −160 mV (Fig. 3*D*). Thus, insertion of a proline for L226 makes the rate of inactivation slower by at least a factor of 10,000.

Although the G219P and L226P mutants are activated by opposite changes in membrane potential, two common effects of these mutations are noteworthy. First, both of these proline substitution mutants are activated by membrane potential changes that are far more negative than WT [52 mV more negative for G219P (Fig. 2*A*), and 123 mV more negative for L226P (Fig. 3*C*)]. Second, both proline-substitution mutations dramatically slow inactivation [1,200-fold for G219P (10), and >10,000-fold for L226P (Fig. 4*D*)]. Thus, proline substitutions at both positions strikingly favor the transition to the open state and strikingly impair the transition to the inactivated state.

**Hyperpolarization Opens the Cytoplasmic Gate of L226P Channels.** Members of the voltage-gated-like ion channel superfamily are thought to open by bending and rotating their S6 (or equivalent M2) transmembrane segments to splay open the bundle of $\alpha$-helices that closes the inner mouth of the pore (7, 10). Is this mechanism of channel opening responsible for the hyperpolarization-activated gating of L226P or is another gating transition involved? We considered two alternative models for L226P gating. (*i*) The pore of L226P might open in response to hyperpolarization by movement of the same cytoplasmic gating mechanism as for depolarization-activated gating of WT. (*ii*) Alternatively, the gating of L226P may be shifted so far in the negative direction that depolarization-activated opening of the

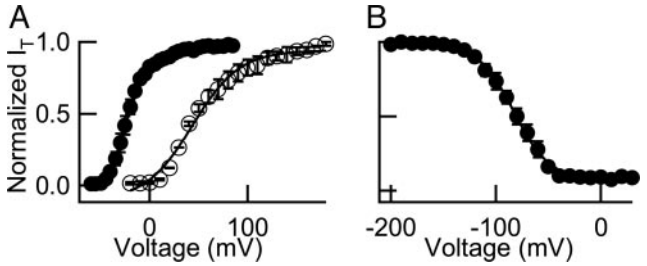


**Fig. 4.** Hyperpolarization-activated $Na^+$ currents of double mutant D60K/L226P. (*A*) Voltage dependence of activation of WT and D60K channels from normalized tail currents. $V_a = -24.0 \pm 1.6$ mV for WT (filled symbols, $n = 7$); $V_a = +51.4 \pm 2.3$ mV for D60K (open symbols, $n = 4$). (*B*) Voltage dependence of activation of D60K/L226P double mutant. Tail currents of the double mutant were measured and plotted as an activation curve as in Fig. 2. $V_a = -83.2 \pm 0.7$ mV ($n = 4$).

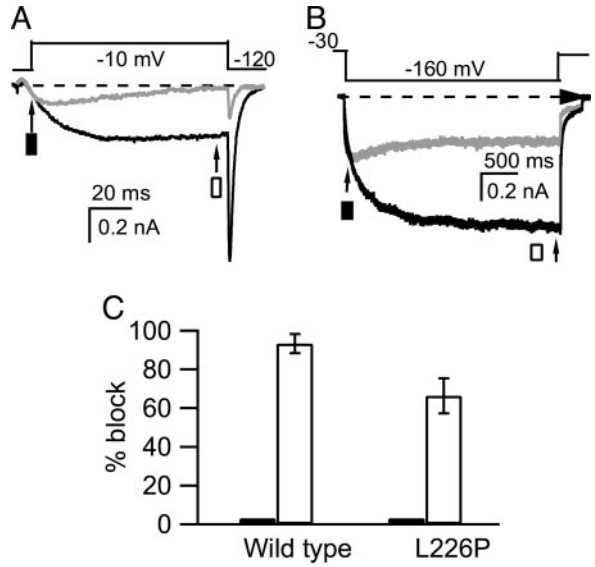


**Fig. 5.** Block of WT and L226P channels by etidocaine. (*A*) WT $Na^+$ currents were evoked by a 100-ms test pulse to −10 mV from a holding voltage of −120 mV before (black trace) and after (gray trace) 200 $\mu$M etidocaine. Dotted line represents zero current. (*B*) L226P $Na^+$ currents were evoked by a 3-s test pulse to −160 mV from a holding voltage of −30 mV before (black trace) and after (gray trace) 500 $\mu$M etidocaine. (C) Time-dependent block of WT and L226P channels by etidocaine. Block of closed channels was estimated at 15 ms for WT and 200 ms for L226P (filled bars; filled rectangles in *A* and *B*). Block of activated channels was measured immediately before the end of the test pulses (open bars; open rectangles in *A* and *B*). Block at the end of the activating pulse was 93.4 ± 5% for WT ($n = 3$) and 66.3 ± 9% for L226P ($n = 3$), respectively.

cytoplasmic gate occurs at potentials more negative than −200 mV, beyond the range of our recording methods. In this case, prolonged depolarization in the range of −200 mV to 0 mV would cause inactivation, and the hyperpolarization-activated gating we observe might be reversal of that inactivation rather than normal pore opening. We used two experimental approaches to test these distinct models.

In a separate series of experiments on voltage sensor mutations, we found that mutation D60K in the S2 transmembrane segment shifts the voltage dependence of activation 75 mV toward depolarizing potentials without other effects on the kinetics or voltage dependence of gating (Fig. 4*A*). Presumably, this mutation disrupts electrostatic interactions of D60 with charged residues in the S4 voltage sensors as observed for voltage-gated potassium channels (21). We reasoned that the combination of this mutation with L226P might result in a double mutant channel (D60K/L226P) with gating in a more positive voltage range. This double mutant began to activate with hyperpolarization beyond −50 mV, and activation reached a clear plateau negative to −130 mV and remained constant to −200 mV (Fig. 4*B*). There was no sign of channel closure upon further hyperpolarization to −220 mV. $V_a$ for this double mutant was −83 mV, ≈64 mV more positive than L226P. Interestingly, introduction of the D60K mutation into L226P causes nearly the same shift in voltage dependence as introduction into WT, despite the fact that L226P opens in response to hyperpolarization and the WT channel opens in response to depolarization. This finding is consistent with the conclusion that the D60K and L226P mutations make additive energy contributions and have independent effects on gating and that the same voltage-sensing mechanism controls depolarization-activated gating in WT and hyperpolarization-activated gating in L226P. The failure of this double mutant to close over the potential range from −130 to −220 where it is fully activated argues against the idea that strongly negatively shifted, depolarization-activated gating is responsible for the open state of the L226P channel, because there are no examples of such widely separated voltage-dependent activation and inactivation processes among the members of the voltage-gated-like ion channel superfamily. Thus, these results favor model *i*, in which the hyperpolarization-activated gating of L226P results from opening of the bundle of S6 helices at the cytoplasmic mouth of the pore.

To probe this question by another approach, we examined block of the channel by the local anesthetic etidocaine, which blocks neuronal $Na^+$ channels by entering the intracellular mouth of the pore and binding to a receptor site formed by the S6 $\alpha$-helices (22–24). Like neuronal $Na^+$ channels, NaChBac is blocked by local anesthetics in a time-dependent manner upon depolarization. For WT, little inactivation is observed during a 100-ms depolarization to −10 mV (Fig. 5*A*). Prior exposure to 200 $\mu$M etidocaine results in a marked change in the time course of the $Na^+$ current in response to depolarization. At early times during the depolarization, there is no difference in the magnitude of the current in the presence of etidocaine (Fig. 5*A*, filled rectangle). As the depolarization continues, the current becomes progressively blocked until, at the end of the pulse, block is nearly complete (Fig. 5*A*, open rectangle). These results demonstrate lack of block of the closed channel at the holding potential followed by time-dependent block of the open channel during the depolarizing pulse. This time-dependent block is consistent with enhanced entry of etidocaine through the open cytoplasmic mouth of the pore and high-affinity binding to its receptor site in the S6 segments during depolarization. We tested whether the same time-dependent block was observed for hyperpolarization-activated gating. For the L226P channel, hyperpolarization to −160 mV for 3 s activates $Na^+$ current with little inactivation. Prior application of 500 $\mu$M etidocaine causes little block at the beginning of the pulse (Fig. 5*B*, filled rectangle), but the $Na^+$ current is progressively blocked as the hyperpolarizing test pulse continues and is blocked by 66% at the end of the pulse (Fig. 5*B*, open rectangle). Block increases similarly during test pulses that cause channel activation for both WT and L226P (Fig. 5*C*), even though the channels are opened by opposite voltage excursions. Thus, as for WT, our results indicate that etidocaine enters the hyperpolarization-activated pore of the L226P mutant and blocks the channel. These results support model *i* for hyperpolarization-activated gating of L226P channels, in which bending splays open the cytoplasmic bundle of S6 helices and opens the pore upon hyperpolarization, similar to the gating of WT in response to depolarization.

Our results with etidocaine block also argue persuasively against model *ii*, in which the increase in $Na^+$ current upon

hyperpolarization of L226P channels reflects reversal of prior channel inactivation. Etidocaine binds most strongly to inactivated $Na^+$ channels (22, 24). Therefore, its binding should be greatest for closed, inactivated L226P channels and should decrease upon hyperpolarization if inactivation is reversed during our test pulses. Our results (Fig. 5) show clearly that drug block increases during the hyperpolarizing test pulses, arguing against $Na^+$ current increase by reversal of inactivation during those pulses. Our results also argue that preferential block of activated channels by local anesthetics like etidocaine depends primarily on the open conformation of the channel as defined by the position of the S6 segments and not by the position of the S4 voltage sensors that are assumed to be opposite for the open states of WT and L226P channels.

**Substitution of Glycine and Histidine for L226 Yields Activation upon Hyperpolarization.** To determine whether substitution of proline is unique in producing a hyperpolarization-activated NaChBac channel, a range of other amino acids were substituted for L226 (Fig. 6). Substitution of methionine, valine, or isoleucine yielded depolarization-activated channels that inactivated during the test pulses like WT (Fig. 6 *Left*). Substitution of alanine, asparagine, phenylalanine, tyrosine, lysine, or cysteine yielded inactive or misfolded channels. Only substitution of glycine or histidine mimicked proline (Fig. 6 *Right*). L226G and L226H produced small but clearly measurable $Na^+$ currents in response to strong hyperpolarizations. Like L226P, these $Na^+$ currents did not inactivate appreciably during the test pulses. Thus, glycine, histidine, and proline at position 226 produce hyperpolarization-activated gating of NaChBac at very negative membrane potentials and prevent inactivation of the channel.

**Bending of S6 Segments Determines Both Voltage Dependence and Polarity of Ion Channel Gating.** Our studies of proline-substitution mutations emphasize the importance of bending of the S6 segments in ion channel gating. Previous x-ray crystallography studies have revealed the structure of the bacterial 2-TM KcsA channels with a bundle of the four M2 $\alpha$-helices crossed at the cytoplasmic end of the pore (5). This structure is proposed to represent the closed state. In contrast, the structure of the distantly related, $Ca^{2+}$-gated MthK channel in the $Ca^{2+}$-bound form has M2 helices that are bent at the position of G219 in NaChBac, and this bend splays open the helical bundle at the cytoplasmic end of the pore (7). This structure is proposed to represent the open state. Our previous studies of the G219P mutant of NaChBac showed that favoring a bend in the S6 segment at position 219 by substitution of proline dramatically enhanced activation gating and stabilized the open state (10). These previous results provide functional support for the model that opening of the pore of the voltage-gated-like superfamily of channels requires a bend in the M2 or S6 segments at the equivalent of position 219 in NaChBac and generalizes this model from the 2-TM bacterial channels studied by x-ray crystallography to the wide range of 6-TM voltage-gated-like channels (10).

The results presented here on proline-scanning mutations that cause hyperpolarization-activated gating extend the evidence that bending of the S6 segment determines the voltage dependence of activation gating. Proline substitutions at three positions in the S6 segment yield hyperpolarization-activated channels. It is striking that these three positions all fall on the same face of the S6 $\alpha$-helix as G219, as illustrated by the helical net in Fig. 1*A Left*. A 100° radial surface of the S6 helix, indicated by shading, contains the positions of all four mutations (Fig. 1*A Left*). Mutations at other positions in the S6 segment give either nonfunctional channels or channels with small changes in gating. We propose that only this face of the S6 helix is available to bend in response to proline substitutions in a way that strongly favors

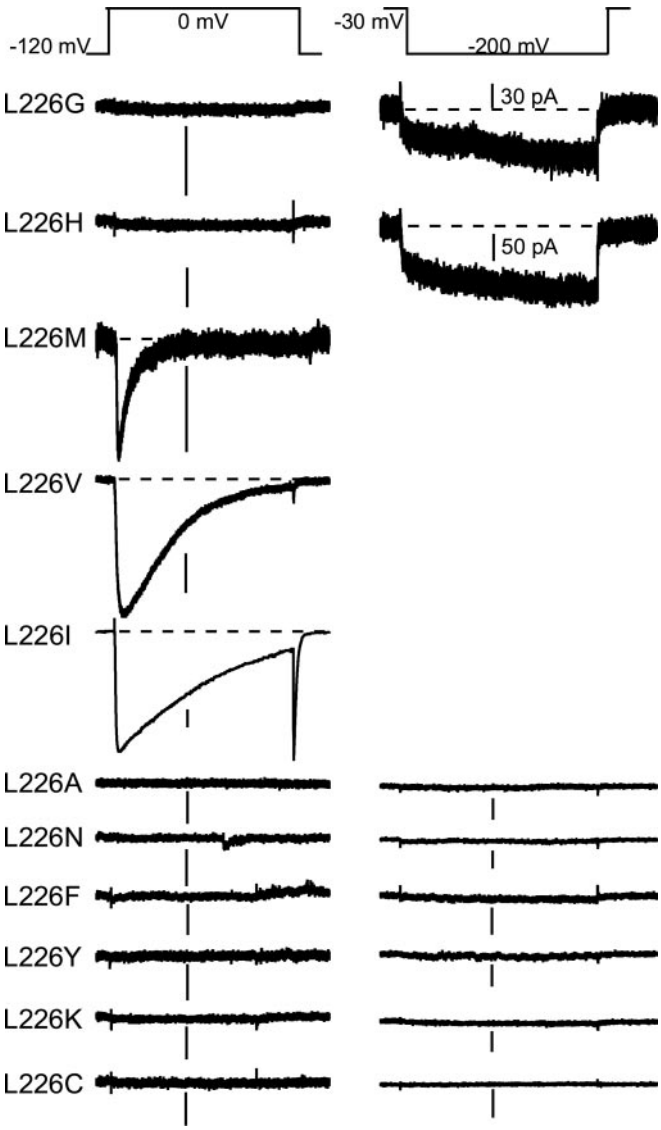


**Fig. 6.** Effects of substitution of other amino acids for L226. Each of the indicated mutant channels was tested by the two protocols for depolarization-activated (*Left*) and hyperpolarization-activated (*Right*) $Na^+$ currents as in Fig. 1. [Scale bars: 0.2 nA (unless otherwise noted).]

opening of the pore and prevents subsequent inactivation. Consistent with this idea, detailed analysis of the G219P and L226P mutations shows that both cause dramatic negative shifts in the voltage dependence of activation gating and dramatic slowing of inactivation. More limited studies of I222P and G229P suggest that the voltage dependence of hyperpolarization-activated gating is dramatically shifted to negative membrane potentials, and inactivation is prevented for them as well (data not shown).

Our results also clearly show that the position of these proline-substitution mutations in the S6 segment determines the polarity of gating. G219P, positioned near the extracellular end of the large cavity in the middle of the pore, causes enhanced depolarization-activated gating. In striking contrast, I222, L226, and G229 are positioned on the same face of the S6 helix but progressively more toward the cytoplasmic end of the pore (Fig. 1*A Left*), and all cause hyperpolarization-activated gating. Evidently, insertion of proline residues toward the intracellular end of this face of the S6 helix dramatically stabilizes the open state

relative to the closed state at negative membrane potentials and, conversely, stabilizes the closed state relative to the open state at positive membrane potentials.

How do proline substitutions cause hyperpolarization-activated gating? Our results do not yet allow a structural interpretation of the mechanism of this reversal of gating polarity. However, our studies of the effects of multiple amino acid residues substituted for L226 support the conclusion that bending at this position is required for hyperpolarization-activated gating of these mutants. Like the WT leucine residue at position 226, valine, methionine, and isoleucine residues have a low turn propensity when in transmembrane $\alpha$-helices (0.4–0.6) (25). Substitution of these amino acid residues for L226 yielded channels with depolarization-activated gating in each case. In contrast, glycine, histidine, and proline residues have much higher turn propensity in transmembrane $\alpha$-helices (1.3, 1.6, and 1.7, respectively), and substitution of these residues for L226 yields hyperpolarization-activated gating. This strong correlation argues that bending of the S6 segment at position 226 is required for hyperpolarization-activated voltage-dependent gating, whereas low turn propensity at that position favors depolarization-activated gating as in WT.

Although it is clear from our results that the L226P mutation is sufficient to produce hyperpolarization-activated gating in NaChBac channels, this is not a uniform property of members of the voltage-gated-like ion channel superfamily. Sequence alignments of the pore-forming segments of all superfamily members (4) show that voltage-gated $K^+$ channels in the $K_V1$ to $K_V9$ families all have a proline residue positioned seven amino acid residues downstream from the proposed hinge glycine in their S6 segments. Despite the position of this proline residue, these channels are activated by depolarization. Moreover, this proline residue is thought to provide an essential bend in the S6 helix that is important for $K_V$ channel gating (26). It will be interesting to determine whether substitution of other amino acid residues at this position in $K_V$ channels can produce hyperpolarization-activated gating.

Our results have clear implications for the hyperpolarization-activated gating of HCN and KAT channels. Studies of the S4 segments of HCN channels has confirmed that they move outward upon depolarization like other voltage-gated channels (27–29), even though HCN channels are activated by hyperpolarization. These results indicate that an alteration in the coupling of outward movement of the S4 voltage sensors to eventual opening of the pore underlies hyperpolarization-activated pore opening in HCN channels. A similar mechanism may cause hyperpolarization-activated gating of KAT channels. In light of our results, it will be important to analyze the S6 segments of animal HCN channels and plant KAT channels to identify amino acid residues that are required for hyperpolarization-activated gating. Such studies may allow construction of point mutants of HCN and KAT channels with reversed polarity of gating as we have demonstrated here for NaChBac.

We thank Dr. Bertil Hille (University of Washington) for critical comments on the manuscript. This work was supported by National Institutes of Health Research Grant RO1 NS15751.

1. Hodgkin, A. L. & Huxley, A. F. (1952) *J. Physiol.* **117,** 500–544.
2. Hille, B. (2001) *Ionic Channels of Excitable Membranes* (Sinauer, Sunderland, MA).
3. Catterall, W. A. (2000) *Neuron* **26,** 13–25.
4. Yu, F. H. & Catterall, W. A. (2004) *Sci. STKE* **2004,** re15.
5. Doyle, D. A., Cabral, J. M., Pfuetzner, R. A., Kuo, A. L., Gulbis, J. M., Cohen, S. L., Chait, B. T. & MacKinnon, R. (1998) *Science* **280,** 69–77.
6. Jiang, Y., Lee, A., Chen, J., Cadene, M., Chait, B. T. & MacKinnon, R. (2002) *Nature* **417,** 515–522.
7. Jiang, Y., Lee, A., Chen, J., Cadene, M., Chait, B. T. & MacKinnon, R. (2002) *Nature* **417,** 523–526.
8. Jiang, Y., Lee, A., Chen, J., Ruta, V., Cadene, M., Chait, B. T. & MacKinnon, R. (2003) *Nature* **423,** 33–41.
9. Ren, D., Navarro, B., Xu, H., Yue, L., Shi, Q. & Clapham, D. E. (2001) *Science* **294,** 2372–2375.
10. Zhao, Y., Yarov-Yarovoy, V., Scheuer, T. & Catterall, W. A. (2004) *Neuron* **41,** 859–865.
11. Cordes, F. S., Bright, J. N. & Sansom, M. S. (2002) *J. Mol. Biol.* **323,** 951–960.
12. Barlow, D. J. & Thornton, J. M. (1988) *J. Mol. Biol.* **201,** 601–619.
13. Zagotta, W. N. & Siegelbaum, S. A. (1996) *Annu. Rev. Neurosci.* **19,** 235–263.
14. Robinson, R. B. & Siegelbaum, S. A. (2003) *Annu. Rev. Physiol.* **65,** 453–480.
15. Ludwig, A., Zong, X., Hofmann, F. & Biel, M. (1999) *Cell. Physiol. Biochem.* **9,** 179–186.
16. Schachtman, D. P., Schroeder, J. I., Lucas, W. J., Anderson, J. A. & Gaber, R. F. (1992) *Science* **258,** 1654–1658.
17. Sentenac, H., Bonneaud, N., Minet, M., Lacroute, F., Salmon, J. M., Gaymard, F. & Grignon, C. (1992) *Science* **256,** 663–665.
18. Margolskee, R. F., McHendry-Rinde, B. & Horn, R. (1993) *BioTechniques* **15,** 906–911.
19. Jurman, M. E., Boland, L. M., Liu, Y. & Yellen, G. (1994) *BioTechniques* **17,** 876–881.
20. Qu, Y., Rogers, J., Tanada, T., Scheuer, T. & Catterall, W. A. (1995) *Proc. Natl. Acad. Sci. USA* **92,** 11839–11843.
21. Papazian, D. M., Shao, X. M., Seoh, S. A., Mock, A. F., Huang, Y. & Wainstock, D. H. (1995) *Neuron* **14,** 1293–1301.
22. Hille, B. (1977) *J. Gen. Physiol.* **69,** 497–515.
23. Yarov-Yarovoy, V., McPhee, J. C., Idsvoog, D., Pate, C., Scheuer, T. & Catterall, W. A. (2002) *J. Biol. Chem.* **277,** 35393–35401.
24. Ragsdale, D. S., McPhee, J. C., Scheuer, T. & Catterall, W. A. (1994) *Science* **265,** 1724–1728.
25. Monne, M., Nilsson, I., Elofsson, A. & von Heijne, G. (1999) *J. Mol. Biol.* **293,** 807–814.
26. Webster, S. M., Del Camino, D., Dekker, J. P. & Yellen, G. (2004) *Nature* **428,** 864–868.
27. Vemana, S., Pandey, S. & Larsson, H. P. (2004) *J. Gen. Physiol.* **123,** 21–32.
28. Bell, D. C., Yao, H., Saenger, R. C., Riley, J. H. & Siegelbaum, S. A. (2004) *J. Gen. Physiol.* **123,** 5–19.
29. Mannikko, R., Elinder, F. & Larsson, H. P. (2002) *Nature* **419,** 837–841.